Medical Image Registration Incorporating Deformations

P. J. Edwards, D. L. G. Hill, J. A. Little, V. A. S. Sahni, D. J. Hawkes
Radiological Sciences
UMDS, Guys Hospital
London SE1 9RT, U.K.
p.edwards@umds.ac.uk

Abstract

Multiple sources of 3D medical image data can be used to construct detailed patient representations. Typically registration is achieved assuming the validity of rigid body transformation. In many applications, and in particular when updating representations used for guidance during surgery and therapeutic interventions, this assumption is inappropriate. In this paper we describe a general method for 3D deformation, show how registration can incorporate a composite of rigid body and deformation components and illustrate this methodology on 3 example sets of images. The first is a repeated 3D MR scan of the abdomen of a volunteer who purposely changed position between scans; the second is an MR and CT scan of the head and neck, in which the patient was in a different position for the two scans; and the third is a set of MR and CT images of the head taken before and after epilepsy surgery. Non rigid deformation and composite warping showed significant improvement in registration accuracy in each case.

1 Introduction

Different medical imaging modalities provide complementary information about pathology, and associated normal anatomy. As a result patients often undergo multiple imaging investigations for diagnosis, planning and more recently guiding interventions. Several computational techniques have been proposed for registering these images into a common coordinate frame in order to provide a more complete representation of the patient [1, 2, 3, 4, 5, 6]. These techniques almost invariably use rigid body transformations. The implicit assumption underlying the use of rigid body registration algorithms is that, to the resolution of the imaging systems, structures of interest in the patient do not deform between image acquisitions. This assumption is normally valid for diagnosis with magnetic resonance (MR), x-ray computed tomography (CT) and nuclear medicine emission tomography (PET or SPECT) images of the brain [1, 3, 5, 6] and, with careful positioning, can also be true for registration of MR or CT with PET or SPECT images of the pelvis [4] and heart [2]. Change in pathology, or movement of structures resulting from surgery or radiotherapy can invalidate the rigid body assumption, even in the brain. Image guided interventions are an important emerging area in minimally invasive therapy. As success is

BMVC 1995 doi:10.5244/C.9.69

dependent on the accuracy of the image representation a means must be found to update rigid body representations in the light of new information, so that the location of critical structures, currently invisible, can be inferred with confidence.

A related application is the "atlas problem" in which images from different individuals are registered to a common coordinate system [1, 7]. Most research into the atlas problem has concentrated on images of the brain. The most widely used algorithms register brain images into a bi-commisural coordinate system, as used by the Talaraich atlas [8]. Various deformation algorithms have been proposed for this problem, including elastic or viscous matching [9, 10] and recent work by Bookstein [11] involving the use of thin plate spline warps. Very little work has been done on single individual registration incorporating deformations either within or outside the brain. An important exception to this is the work of Mardia [12], in which x-ray projections have been registered to nuclear medicine planar bone scans of the spine using kriging.

In this paper we describe work in progress in which a variety of 3D warping algorithms have been applied to the registration of example images of the head, neck and spine from MR and CT, and of pre-operative and post-operative images of the brain. We present initial results combining rigid body registration and non-rigid deformations.

2 Method

If equivalent points can be identified in two images of the same object, these points can be used to determine the geometric transformation relating the two images. The registration algorithm can be rigid body, or incorporate deformations.

2.1 Rigid Body Registration

We determine the rigid body transformation relating the coordinate system of two separate images using an algorithm which decouples translations and rotations, proposed by Arun [13]. The translation component of the transformation is determined by aligning the centroids of the two pointsets. Singular value decomposition (SVD) is then used to determine the rotation transformation which minimises the sum of square displacements between corresponding points.

2.2 Registration incorporating deformations

Point based interpolation techniques interpolate from $\mathbb{R}^d$ to $\mathbb{R}$, that is given a set of points in d-dimensional space each with a given value then they form an interpolator which is exact at this point and smooth elsewhere. Solutions to this problem arise when minimising a penalty function with respect to the mapping. A general penalty function for splines is given by, see Wahba [14],

$$J_m^d(\Phi) = \sum_{\alpha[1]+\cdots+\alpha[d]=m} \frac{m!}{\alpha[1]!\cdots\alpha[d]!} \int_{-\infty}^{\infty} \cdots \int_{-\infty}^{\infty} \left(\frac{\partial^m \Phi}{\partial t[1]^{\alpha[1]} \cdots \partial t[d]^{\alpha[d]}} \right)^2 \prod_j dt_j, \tag{1}$$

where m is the order of the derivatives used. The two dimensional solution for $m = 2$ is well known and is the thin-plate spline, [15]. Let us have n sites represented by $\mathbf{t}_i =$

$(t_i[1], t_i[2])^T$, $i = 1, \ldots, n$ with required values x_i. The solution for the whole of $\mathbb{R}^2$ can now be given as,

$$f(\mathbf{t}) = a_1 + a_2 t[1] + a_3 t[2] + \sum_{j=1}^{n} b_j \sigma(\mathbf{t} - \mathbf{t}_j), \tag{2}$$

with coefficients given by

$$\begin{pmatrix} \Sigma & D \\ D^T & 0 \end{pmatrix} \begin{pmatrix} \mathbf{b} \\ \mathbf{a} \end{pmatrix} = \begin{pmatrix} \mathbf{x} \\ 0 \end{pmatrix}. \tag{3}$$

where

$$\begin{aligned} (\Sigma)_{ij} = \sigma(\mathbf{t}_i - \mathbf{t}_j) = |\mathbf{t}_i - \mathbf{t}_j|^2 \log |\mathbf{t}_i - \mathbf{t}_j|, \ \mathbf{b}^T = (b_1, \ldots, b_n), \\ \mathbf{a}^T = (a_1, a_2, a_3), \ \mathbf{x}^T = (x_1, \ldots, x_n), \end{aligned} \tag{4}$$

and the ith row of D is $(1, t_i[1], t_i[2])$.

Point based image warping algorithms operate by matching two sets of landmark or control points exactly and then interpolating throughout the rest of the image.

Let us have two sets of corresponding 3D points given by $\mathbf{t}_i^T = (t_i[1], t_i[2], t_i[3])$ and $\mathbf{u}_i^T = (u_i[1], u_i[2], u_i[3])$, $i = 1, \ldots, n$ and call these the original and new landmarks respectively. We wish to deform our image so that landmark $\mathbf{t}_i$ moves to a new position $\mathbf{u}_i$ for all n landmarks and then to interpolate the remainder of the image subject to these constraints.

A three dimensional deformation can be achieved by using three independent interpolators from $\mathbb{R}^3 \rightarrow \mathbb{R}$ to model the displacement of the $t[1]$, $t[2]$ and $t[3]$ ordinates independently. We shall call these solutions $f_1(\mathbf{t})$, $f_2(\mathbf{t})$ and $f_3(\mathbf{t})$ respectively. Using the constraints,

$$f_1(\mathbf{t}_i) = u_i[1], \ f_2(\mathbf{t}_i) = u_i[2], \ f_3(\mathbf{t}_i) = u_i[3], \tag{5}$$

we can now define a deformation for any point in the plane by

$$\mathbf{t} \rightarrow (u[1], u[2], u[3])^T = (f_1(\mathbf{t}), f_2(\mathbf{t}), f_3(\mathbf{t}))^T. \tag{6}$$

This will be an exact interpolant for the landmarks $\mathbf{t}_i$ and a smooth deformation elsewhere.

Solutions to this problem, using splines, radial basis functions and kriging, are well known, [14, 16, 12], and take the following form

$$f_l(\mathbf{t}) = a_1[l] + a_2[l] t[1] + a_3[l] t[2] + a_4[l] t[3] + \sum_{j=1}^{n} b_j[l] \sigma(\mathbf{t} - \mathbf{t}_j), \ l = 1, 2, 3. \tag{7}$$

With coefficients given by the solution of the following system of linear equations,

$$\begin{pmatrix} \Sigma & D \\ D^T & 0 \end{pmatrix} \begin{pmatrix} \mathbf{b}_1 & \mathbf{b}_2 & \mathbf{b}_3 \\ \mathbf{a}_1 & \mathbf{a}_2 & \mathbf{a}_3 \end{pmatrix} = \begin{pmatrix} \mathbf{u}_1 & \mathbf{u}_2 & \mathbf{u}_3 \\ 0 & 0 & 0 \end{pmatrix} \tag{8}$$

where

$$\begin{aligned} (\Sigma)_{ij} = \sigma(\mathbf{t}_i - \mathbf{t}_j), \ \mathbf{b}_l^T &= (b_1[l], \ldots, b_n[l]), \ \mathbf{a}_l^T = (a_1[l], \ldots, a_4[l]), \\ \mathbf{u}_l^T &= (u_1[l], \ldots, u_n[l]), \ l = 1, 2, 3. \end{aligned} \tag{9}$$

and the ith row of D is $(1, t_i[1], t_i[2], t_i[3])$. In this paper the basis function used is $\sigma(\mathbf{t}_i - \mathbf{t}_j) = |\mathbf{t}_i - \mathbf{t}_j|$. This is the three dimensional analogy of the thin-plate spline.

2.3 Registration incorporating rigid body and deformation components

The human body contains many discrete structures, with different mechanical, plastic, elastic and viscous properties. Some of these structures are rigid, others deform to varying degrees. In an initial study of this problem, we have developed a composite registration algorithm in which these different structures can be treated separately. One image, the "reference image", is left in its original form. The second image is segmented into structures that are rigid and structures that deform. We then construct a linear deformation to map the rigid structures from this second image into the reference image coordinate frame, and a non-linear deformation to map the deformable structures into the reference frame. Both these procedures involve point matching algorithms, so 3D landmarks are separately identified in the rigid and deformable structures in the images.

The rigid portions of the image are registered using the method outlined in section 2.2, and the deformable portions using equations (6)-(9). Once these portions of the image have been separately transformed, they are recombined. Voxels at structure boundaries can be assigned multiple values in the final coordinate frame. We currently arbitrarily assign these image voxels with the value from the deformed structure.

2.4 Clinical application 1: images of the spine.

A normal volunteer was positioned in a 1.5 Tesla MR scanner (Philips Gyroscan ACS II), and imaged with a T1 weighted sagittal sequence using a dedicated spine coil. They were then removed from the scanner, repositioned and re-imaged. 3D points were identified in the two datasets, and these were used to register the images using the individual rigid body and warping transformations described above. For both transformation calculations a set of 46 landmarks on the vertebrae were used.

2.5 Clinical application 2: images of the neck

The same approach was used to register clinical MR and CT images from a patient with a parotid tumour. 12 points were identified in the base of the brain. These were used to register the images using the rigid body transformation. A further 10 points were identified in the neck and the warping algorithm was used.

2.6 Clinical application 3: images of the brain

The adult brain, due to physical containment by the skull, normally behaves like a rigid structure, to the resolution of radiological imaging. During surgery, however, the brain can change shape significantly. Clinical images were selected from a patient whose brain had changed shape dramatically as a result of an operation to implant subdural electrode mats. During the operation, a surgical guidance system, incorporating a mechanical arm localiser, had been used to register the preoperative MR images to surgical coordinates. At the time the electrodes were implanted, measurements made with the arm indicated that, to the accuracy of the system, the brain surface was in the same position, relative to the skull, as it had been in the preoperative MR images. The positions of the electrodes were also recorded using the localiser. Post-operatively, a CT scan was acquired. This indicated that the brain surface underneath the craniotomy had shrunk so that, in some places, the

surface of the brain was more than 10mm inside the skull. The electrodes, clearly visible in the CT scan, were attached to the outer surface of the brain. The contralateral hemisphere appeared unchanged.

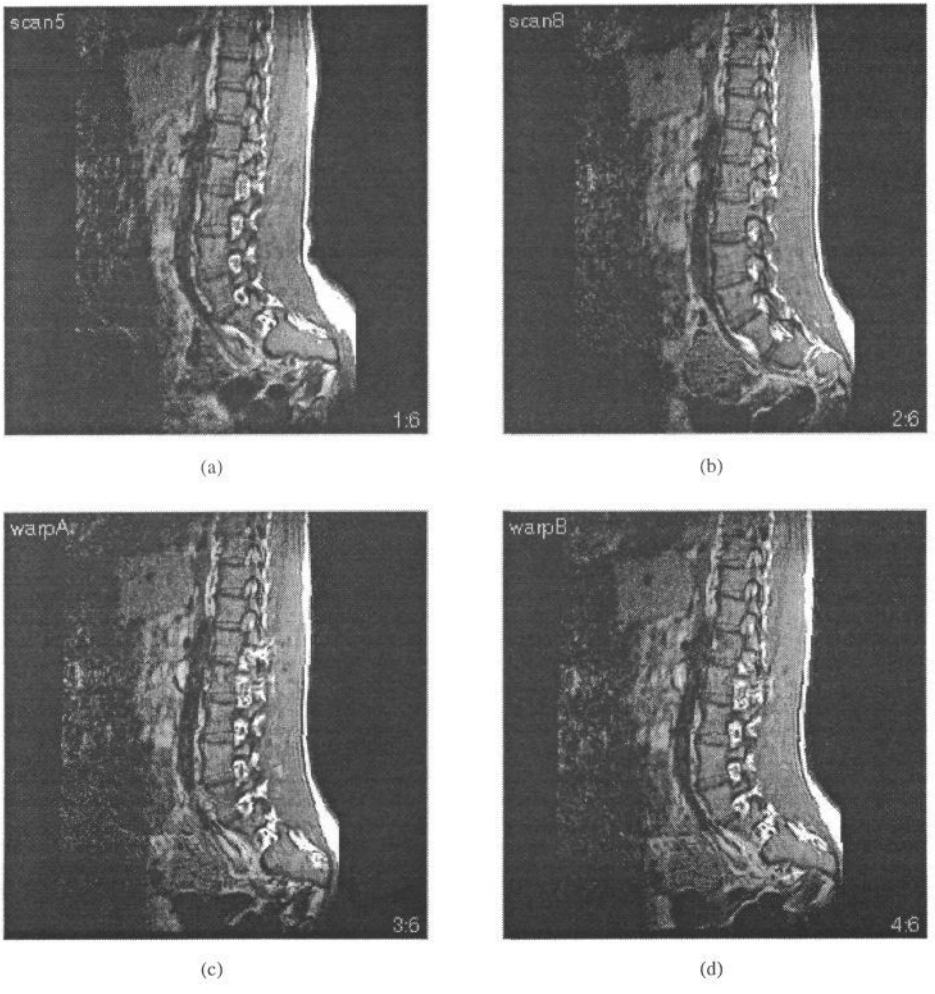

Figure 1: Comparison of rigid body and 3D warping on a MR image of the spine, (a) Original MR image, (b) New MR image after movement, (c) the result of transforming (b) to (a) using rigid body transformation and (d) the result of transforming (b) to (a) using 3D warping. Warping provided a more accurate estimate of the position of the lumbar spine and abdominal aorta.

Twelve anatomical landmarks, and the eight centres of the electrodes were used as registration points. These were used to calculate a rigid body and non-linear warp to transform the entire pre-operative MR image into the coordinate frame of the post-operative CT image. The composite registration algorithm described in section 2.3 was also used to treat the shrunken hemisphere separately from the remainder of the head. The hemisphere was first segmented from the preoperative MR image. The coordinates of the electrodes,

and additional points on the mid-line were used to calculate a warping transformation for this hemisphere alone. The remainder of the preoperative MR image was transformed into postoperative CT coordinates using a rigid body transformation calculated from anatomical landmarks outside of the shrunken hemisphere. The rigidly transformed and warped portion of the MR image were then recombined into a single image volume.

3 Results

3.1 Clinical application 1: spine

Figure 1 shows example sagittal sections from a volume image of a volunteer's spine. Figure 1(a) shows the spine in position 1; figure 1(b) shows the spine in position 2; figure 1(c) shows the least squares 3D rigid transformation of 1(b) to the coordinates of 1(a). Figure 1(d) shows the result of applying equations (6)-(9) using the same landmarks used to produce figure 1(c). Figure 1(d) is much more like figure 1(a), than is figure 1(c). For example, the course of the lumber spine and aorta are clearly incorrect in 1(c).

3.2 Clinical application 2: neck

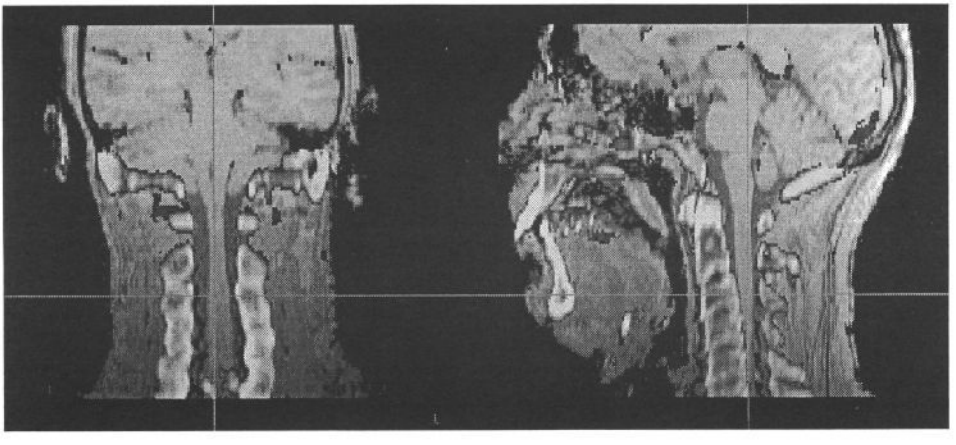

Figure 2: Rigid body image registration of an MR and CT image pair, white-CT, grey level-MR, showing two orthogonal slices through the neck. Left is the coronal or side-to-side slice and right is the sagittal or front-to-back slice . The cut planes are indicated by the cross hairs.

Figures 2 and 3 show reformatted orthogonal sections from a combined MR and CT dataset of a patient with a parotid tumour. Figure 2 was produced by applying a 3D rigid body transformation to the CT using landmarks identified in the skull base. Note that the spinal cord from MR appears to overlap with the spine from CT in the sagittal section. At the bottom of the coronal section the spine can be seen protruding into the space occupied by the spinal cord. Figure 3 was produced by applying equations (6)-(9) using these same landmarks. Notice that the brain appears unchanged, but the CT bone is now correctly orientated relative to the spinal cord from MR.

Figure 3: Non-linear image registration of the same MR and CT image pair as shown on figure 2.

3.3 Clinical application 3: brain

Figure 4 shows example axial slices from a patient who underwent neurosurgery for the implantation of subdural electrodes. Figure 4(a) shows the postoperative CT scan. Note the electrodes clearly visible on the surface of the brain and in the interhemispheric fissure. It is clear, by comparing this image with the corresponding preoperative MR slice (4(b)), that the left hemisphere of the brain (right side of the image) has shrunk between the MR and CT acquisitions, and fallen away from the inner surface of the skull. Figure 4(b) was aligned with figure 4(a) using a rigid body transformation. Figure 4(c) was produced by warping the preoperative MR image to the postoperative CT image using equations (6) to (9) on the whole image volume. Figure 4(d) was produced by applying equations (6) to (9) to the left hemisphere, and rigid body transformation to the remainder. In figure 4(c), the left hemisphere of the brain was warped approximately correctly, but this led to clinically implausible distortion of the extracranial portions of the image. In producing figure 4(d), the rigidy of the skull was maintained by applying the rigid body transformation to the extracranial parts of the image.

4 Discussion

We have demonstrated the need for non-linear transformations when registering images of the spine, and images acquired before and after operations. In the spine application, 3D warping techniques can produce results that appear more visually satisfactory than the rigid body transformation. Warping algorithms smoothly deform an image, no matter how anatomically incorrect this is. We demonstrated in the brain example, that this can result in implausible deformation of rigid anatomical structures. To overcome this limitation, we have developed a composite approach in which an image is segmented into separate structures that can be transformed independently, and then recombined. Initial results in-

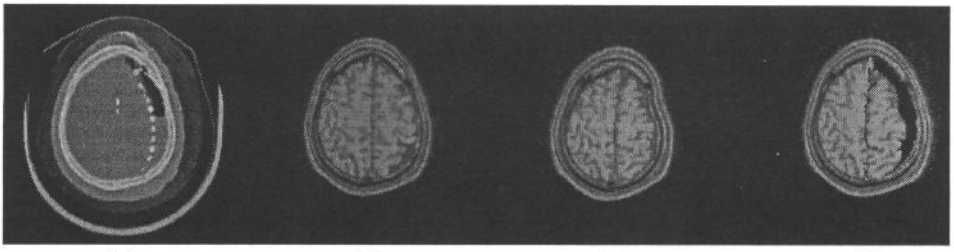

(a) (b) (c) (d)

Figure 4: Non-linear and composite warping of MR and CT images of the head (a) post-operative CT, (b) preoperative MR, (c) 3D warping of the MR to the CT and (d) combined rigid body and 3D warping of the MR to the CT.

dicate that the combined approach is more satisfactory than either the rigid transformation or warping alone.

This paper reports work in progress and it is clear that a more rigorous approach to the treatment of boundaries between rigid and deforming structures is necessary. The simple composite algorithm does not provide continuity at these boundaries as we arbitrarily chose the voxel value from the warped structure. We are working on a single algorithm that will provide such continuity and treat some portions of the image as rigid structures, while warping other portions. A third type of structure which has no energy associated with bending (e.g. fluid filled spaces) should also be incorporated. It is also necessary to distinguish between adjacent structures that are physically attached at their boundary, and adjacent structures that can slide past each other or become detatched.

5 Acknowledgements

The work in this paper was funded by the UK EPSRC, and Philips Medical Systems. We are grateful to our clinical collaborators Professor Andreas Adam, Dr. Alan Colchester, Dr. Tim Cox, Prof. Michael Gleeson, Mr. Charles Polkey, and Mr. Anthony Strong for their continuing support, and to the radiography staff at the Guy's and St Thomas' NHS Trust, and the Maudsley Neurosurgical Centre.

References

[1] A. C. Evans, S. Marrett, J. Torrescorzo, S. Ku, and L. Collins. MRI-PET correlation in three dimensions using a volume-of-interest (VOI) atlas. *J. Cereb. Blood Flow Metab.*, 11:A69–A78, 1991.

[2] T. L. Faber, R. W. McColl, R. M. Opperman, J. R. Corbett, and R. M. Pesnock. Spatial and temporal registration of cardiac SPECT and MR images. methods and evaluation. *Radiology*, 179:857–861, 1991.

[3] D. L. G. Hill, D. J. Hawkes, J. E. Crossman, M. J. Gleeson, T. C. S. Cox, E. E. C. M. L. Bracey, A. J. Strong, and P. Graves. Registration of MR and CT images for

skull based surgery using point-like anatomical features. *The British Journal of Radiology*, 64:1030–1035, 1991.

[4] C. R. Meyer, G. S. Leichtman, J. A. Brunberg, R. L. Wahl, and L. E. Quint. Simultaneous use of homologous points, lines and planes for optimal 3D linear registration of multimodality imaging data. *IEEE trans. Med. Imag.*, 14:1–11, 1995.

[5] C. A. Pelizzari, K. K. Tan, D. N. Levin, G. T. Y. Chen, and J. Balter. Interactive 3D patient patient-image registration. In A. C. F. Colchester and D. J. Hawkes, editors, *Information Processing in Medical Imaging*, pages 133–141. Heidelburg: Springer Verlag, 1991.

[6] U. Pietrzyk, K. Herholz, and W-D. Heiss. Three dimensional alignment of functional and morphological tomograms. *J. Comput. Assist. Tomogr.*, 14:443–457, 1990.

[7] K. J. Friston, C. D. Frith, P. F. Liddle, and R. S. J. Frackowiak. Plastic transformation of PET images. *J. Comput. Assist. Tomogr.*, 15:635–639, 1991.

[8] J. Talairach and P. Tournoux. *A coplanar stereotaxic atlas of a human brain*. Thieme, Stuttgart, 1988.

[9] R. Bajcy and S. Kovacic. Multiresolution elastic matching. *CVGIP: Graphical Models and Image Processing*, 46:1–21, 1989.

[10] C. A. Christensen, R. D. Rabbitt, M. I. Miller, S. C. Joshi, U. Grenader, A. Coogan, and D. C. Van Essen. Topological properties of smooth anatomic maps. In Y. Bizais, C. Barillot, and R. Di Paola, editors, *Information Processing in Medical Imaging*, pages 101–112. Kluwer Academic Publishers, 1995.

[11] F. L. Bookstein. Thin-plate splines and the atlas problem for biomedical images. In A. C. F. Colchester and D. J. Hawkes, editors, *Information Processing in Medical Imaging*, 1991.

[12] K. V. Mardia and J. A. Little. Image warping using derivative information. In F. L. Bookstein, J. S. Duncan, N. Lange, and D. C. Wilson, editors, *Mathematical Methods in Medical Imaging III*, pages 16–31. SPIE Proceedings 2099, July 1994.

[13] K. S. Arun, T. S. Huang, and S. D. Blostein. Least squares fitting of two 3-D point sets. *IEEE Trans. PAMI*, 9(5):698–700, 1987.

[14] G. Wahba. *Spline Models for Observational Data*. Philadelphia: Society for Industrial and Applied Mathematics, 1990.

[15] F. L. Bookstein. Principal warps: thin-plate splines and the decomposition of deformations. *IEEE Trans. PAMI*, 11:567–585, 1989.

[16] N. Arad, N. Dyn, D. Reisfeld, and Y. Yeshurun. Image warping by radial basis functions: Application to facial expressions. *CVGIP: Graphical Models and Image Processing*, 56(2):161–172, March 1994.